The Stability Analysis and Control Strategies of Multiparalleled SAPFs: A Comprehensive Overview

Zhaokang Wu, Guoqing Xu, *Senior Member, IEEE*, Wei Zhu, and Gang Sheng

***Abstract*—An active power filter (APF) is a power electrical equipment that possesses the functions of harmonic suppression and reactive power compensation in the power grid. Its performance is closely related to the adopted topology, harmonic current detection techniques, and harmonic current control methods. In order to promote the use of APF technology in a wider range of industrial applications, we first compare several commonly used APF techniques and highlight the advantages of a shunt active power filter (SAPF) in high-capacity applications. Then, we summarize the harmonic current detection techniques, harmonic current control techniques, and resonance suppression techniques of a single SAPF module and comprehensively compare the merits and demerits of various algorithms. Based on the technologies related to a single SAPF, we introduce the modeling and stability analysis methods of the multiparalleled SAPF system and discuss the existing problems from multiple perspectives. Finally, we provide a detailed description of parallel operation strategies of multiparalleled SAPFs, highlight the advantages, disadvantages, and application scope of various schemes, and prospect the future development of this field.**

***Index Terms*—Control strategies, harmonic suppression, modeling and stability analysis, multiparalleled shunt active power filters (SAPFs), parallel operation strategies.**

I. Introduction

In 1969, Bird et al. [1] proposed the essential principle of active power filters (APFs) as a means to eliminate harmonics within electrical power systems. The method involves injecting compensation currents or voltages into the grid, which have the same amplitude and opposite direction compared to the harmonic loads, in order to make the overall harmonic currents or voltages in the power system zero. This technology can be categorized into shunt active power filters (SAPFs), series APFs [2], [3], and unified power quality conditioner [4] that incorporate both the topologies. However, the latter two solutions require different transformer designs for different types of load, making them less versatile. The SAPF is widely used due to its simplicity and ease of expansion [5], [6]. By the 1990s, APFs were widely applied in countries with advanced power technologies, and companies such as Siemens and ASEA Brown Boveri had produced reputable APF engineering products. Due to extensive research on APF circuit topologies, the majority of APF engineering applications now rely on three-level neutral-point-clamped (NPC) inverters with LCL filters. The research focus has shifted toward harmonics detection [7], current control algorithms [8], and capacity-boosting techniques [9], [10].

Scientists and engineers have proposed various schemes, such as hybrid active power filters (HAPFs) [11], [12], modular multilevel active power filters (MMCAPFs) [13], [14], and multiplex strategies for the main circuits [15] and multiparalleled SAPFs [16], [17], to enhance the output capacity of APFs. The characteristics and limitations of the first three options are listed as follows.

1) The HAPF is composed of a passive power filter (PPF) and an APF, among which the PPF primarily eliminates fundamental reactive power and low-frequency harmonic components and the APF mainly compensates high-frequency harmonic components. Compared with the conventional APF, its capacity of the active part is considerably diminished, so we can employ this approach in larger power situations. However, this scheme lacks generality and portability in different grid impedances and harmonic loads, and the PPF part is easy to resonate with the harmonic components in the power system.
2) The MMCAPF offers advantages, such as high modularity, multilevel pulsewidth modulation (PWM) waveform output, and the ability, to increase voltage levels easily. However, it is suitable mainly for high-voltage and high-power applications, and not for low-voltage and high-power situations. In addition, the problem of circulating currents among modules persists in cases of three-phase voltage unbalance and remains a significant challenge to overcome.
3) Although the multiplex strategy for the main circuits could minimize the total capacitance in the dc link, each module of this scheme shares a set of capacitors, which results in low dependability.

The most common industrial configuration for APFs is the multiparalleled SAPF, which is superior for boosting system capacity in low-voltage and high-power applications when compared to the earlier schemes. As shown in Fig. 1, this method often involves several SAPF modules with uniform specifications and parallel connections between each output of modules, offering the following notable advantages.

Manuscript received 8 March 2023; revised 18 July 2023; accepted 4 August 2023. Date of publication 11 August 2023; date of current version 19 April 2024. This work was supported in part by National Key R&D Program of China under Grant 2018YFB0104803. Recommended for publication by Associate Editor Marta Molinas. *(Corresponding author: Guoqing Xu.)*

Zhaokang Wu, Guoqing Xu, and Wei Zhu are with the School of Mechatronic Engineering and Automation, Shanghai University, Shanghai 200444, China (e-mail: wuzhaokang@shu.edu.cn; gqxu@shu.edu.cn; zhuwei@nancal.com).

Gang Sheng is with Nancal Electric, Shanghai 201210, China (e-mail: shenggang@nancal.com).

Color versions of one or more figures in this article are available at https://doi.org/10.1109/TPEL.2023.3304379.

Digital Object Identifier 10.1109/TPEL.2023.3304379

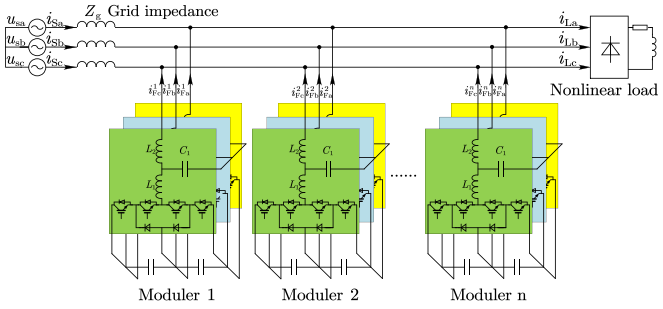

Fig. 1. Structure of the multiparalleled SAPFs.

1) Because usually the parameters are the same for each module, it is very convenient for mass production in this scheme.
2) There is a significant benefit over other alternative plans if on-site maintenance is necessary, such as replacing broken modules and momentarily increasing capacity.
3) Redundancy control is easy to implement in this scheme. To maintain the system functioning properly in the case of a module failure or damage, we can immediately deactivate the damaged module and activate the redundant module.

Numerous studies have been conducted for multiparalleled SAPFs. However, the available research is relatively fragmented and lacks comprehensive descriptions. Based on the stability analysis and control strategy, we present a comprehensive literature survey to classify and summarize the existing technologies, with a deep analysis to their application conditions, compensation effect, cost, reliability, and the development prospects of multiparalleled SAPFs.

The rest of this article is organized as follows. In Section II, we organize the control strategies of a single SAPF module, including its harmonic detection, current control algorithm, and resonance damping strategy. In Section III, based on the modeling and stability analysis of multiparalleled structure, we categorize technologies of the resonance suppression and propose future research directions. Then, in Section IV, we carry out a detailed study on the progress and outstanding problems of control strategies of multiparalleled SAPFs and compare the advantages and disadvantages of the various options. Finally, Section V concludes this article and discusses future research directions in this field, providing valuable insights for further studies.

II. Control Strategies of a Single SAPF

The study of control strategies for a single SAPF serves as the foundation for the research on multiparalleled SAPFs. In this section, we provide a detailed description of the current detection, current control algorithm, and resonance suppression.

A. Harmonic Detection and Current Control Algorithm

The methods for detecting harmonics that are often employed in SAPFs are shown in Fig. 2; we primarily categorize them into frequency and time domains. The most widely used method in

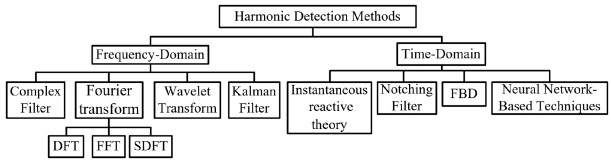

Fig. 2. Classification of common harmonic detection techniques.

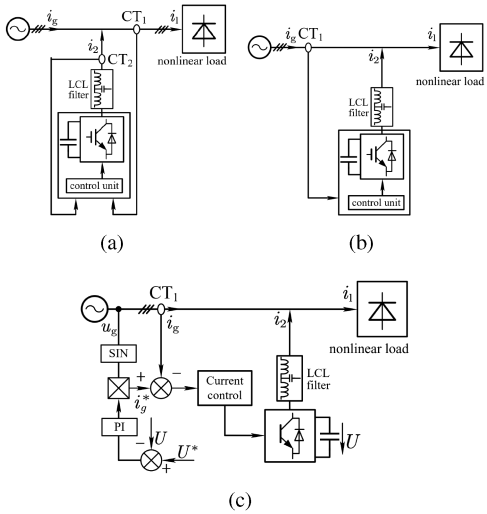

Fig. 3. Classification according to the location of CTs. (a) Open-loop control. (b) Closed-loop control. (c) DCC.

the time domain is the ip-iq approach based on instantaneous reactive theory [18], [19], which has the advantages of quick dynamic response and insensitivity to grid voltage distortion. It was improved by Zhou et al. [20] so that it can be applied to single-phase systems and extract particular order harmonics. On the other hand, the Fourier transform (FT) is the most popular frequency-domain technique [21], [22]. It is generally accepted that the discrete Fourier transform (DFT) is better suited for SAPFs than the fast Fourier transform (FFT) [23], while the FFT is more widely used in actual engineering applications because the digital signal processor can directly implement the FFT through internal library functions. The spectral leakage and picket fence effect are two persistent issues of the FT; the former may be mitigated by employing reasonable window functions [24] and the latter by using interpolation algorithms [25]. Furthermore, techniques, such as the complex filter [26], Kalman filter [27], wavelet transform [28], etc., can be used for harmonic detection; however, due to the algorithm's complexity, slow dynamic response, and excessive computation, they are more suitable for offline detection than APF applications with strict real-time requirements.

According to the position of the current transformer (CT) installation, Fig. 3(a) and (b) illustrates that the control mechanism of APFs may be categorized into open- [29] and closed-loop controls [30], [31]. The term "open-loop control" refers to the sampling and feedback regulation of the nonlinear load current i_L, which has benefits of fast dynamic response and easy implementation of power device protection. On the other hand, closed-loop control, which directly regulates grid current i_s,

theoretically has advantage of requiring fewer current sensors. However, it has a slower dynamic response, which is prone to current overshoot and has a negative impact on power device protection. Therefore, it is difficult to apply in practical device systems, and open-loop control is currently employed by the great majority of SAPFs. In addition, in [32] and [33], it was found under the conditions of proportional–integral (PI) control that open-loop control has lower steady-state accuracy compared with closed-loop control, while their stability is the opposite. However, there are few reports comparing open- and closed-loop controls for other types of current control algorithms. As shown in Fig. 3(c), a method called direct current control (DCC) is proposed [34]. The controlled member in this method is still the grid current i_s, so it can be considered as a variation of closed-loop control. The difference between DCC and the traditional closed-loop control lies in its control objective, which is a sine wave obtained by multiplying the output of PI control of the dc-side voltage with the grid-side voltage. Therefore, DCC does not require harmonic detection algorithms, but it is unable to compensate for harmonic currents in a frequency-dependent manner.

Traditional PI control does not work well for SAPFs since the harmonic currents being regulated comprise sine waves with different frequencies [35]. In order to make the output current of SAPFs quickly and accurately track the given value that is calculated by harmonic current detection, scholars have suggested a number of high-performance harmonic current control techniques, such as the repetitive control (RC) [36], [37], proportional resonant (PR) [38], [39], and vector proportion–integral (VPI) [31] controller based on the internal model principle [41], [42], which includes the mathematical model of the controlled object, so internal model controllers could provide high gain for each order of command harmonic currents and follow them with a small static error in principle. In addition, research in this field also focuses on more complex algorithms, such as deadbeat control (DBC) [43], [44], sliding-mode control (SMC) [45], [46], model-predictive control (MPC) [47], [48], and intelligent control. The combination of DBC and internal model control is often used to improve the steady-state accuracy of traditional deadbeat algorithms [49], [50]. In terms of intelligent control algorithms, fuzzy algorithms [51], particle swarm algorithms [52], and neural network algorithms are currently being studied more extensively, and they are often combined with SMC [53], [54], [55] to improve dynamic response time and reduce the steady-state error. However, intelligent control is often challenging to implement on mainstream digital processors due to its complex algorithms. Typically, the feasibility of intelligent control algorithms is verified through simulation or semiphysical simulation platforms, such as dSPACE [53], [54]. In practical industrial applications, we place more emphasis on the steady-state accuracy rather than the dynamic response. Moreover, we prefer control algorithms that are simple and reliable. Therefore, PI+PR/RC control and its improved algorithms dominate the field. As a consequence, in the ongoing study involving harmonic current control, in addition to enhancing the dynamic and static performance of the proposed control methods, we also need to give more thought to how practicable it would be to apply them. Then, Table I illustrates the merits and demerits of various current control algorithms, and it should be noted that the performance indicators mentioned in Table I are relative to traditional PI control.

TABLE I
COMPARISON OF VARIOUS CONTROL ALGORITHMS

Control algorithm	Merit	Demerit
SMC	1. Fast dynamic response 2. Strong anti-interference 3. Simple structure	1. Chattering phenomenon 2. Parameter tuning is difficult
MPC	1. Fast dynamic response 2. Multi-objective optimization	1. Accurate mathematical model is needed 2. Complicated calculation 3. Parameter tuning is difficult
PI+PR	High steady accuracy	1. Slow dynamic response 2. Complicated calculation 3. Parameter tuning is difficult
PI+RC	1. High steady accuracy 2. Parameter tuning is simple 3. Simple structure	Slow dynamic response
PI+VPI	High steady accuracy	1. Slow dynamic response 2. Complicated calculation 3. Parameter tuning is difficult 4. Cannot compensate zero sequence current
RC+DBC	1. High steady accuracy 2. Relatively fast dynamic response	Sensitive to system parameter

B. Technologies of Impedance Reshaping and Resonance Suppression

Large-capacity SAPFs generally employ LCL-type filters to generate output waveforms that are smoother, although the LCL network causes a resonance phenomenon near to the control stability boundary [56], [57]. The remodeling of the inner output impedance Z_o and the outer output impedance Z_o' of the SAPF circuit model is the essence of the resonance suppression approaches described below. To adjust the inner output impedance, the most common approach is passive damping (PD) [58], [59]. Fig. 4(a) shows a total of six fundamental PD structures. However, this method incurs extra resistance losses. As illustrated in Fig. 4(b)–(d), active damping (AD) techniques may be employed to remove this resistance loss [60], [61], including AD based on state feedback (such as inverter-side current feedback [62], [63], grid-side current feedback [64], [65], capacitor current feedback [66], [67], and capacitor voltage feedback [68]), notch filters [69], [70], and auxiliary active damper circuit [71]. In Fig. 4(b), assuming that the LCL filter has no damping resistance, so $G_{i1}(s)$, $G_{i2}(s)$, $G_{iC}(s)$, and $G_{uC}(s)$ are the ideal transfer functions from inverter output voltage u_{inv} to inverter-side current i_1, grid-side current i_2, capacitor current i_c, and capacitor voltage u_c, respectively, and $G_{\text{ad\_}x}(x = i_1, i_2, iC, \text{ and } uC)$ are the feedback transfer functions to increase damping actively, which are given as

$$G_{i1}(s) = \frac{i_1(s)}{u_{\text{inv}}(s)} = \frac{1}{sL_1}\frac{s^2+\omega_a^2}{s^2+\omega_r^2} \tag{1}$$

$$G_{i2}(s) = \frac{i_2(s)}{u_{\text{inv}}(s)} = \frac{1}{sL_1}\frac{\omega_a^2}{s^2+\omega_r^2} \tag{2}$$

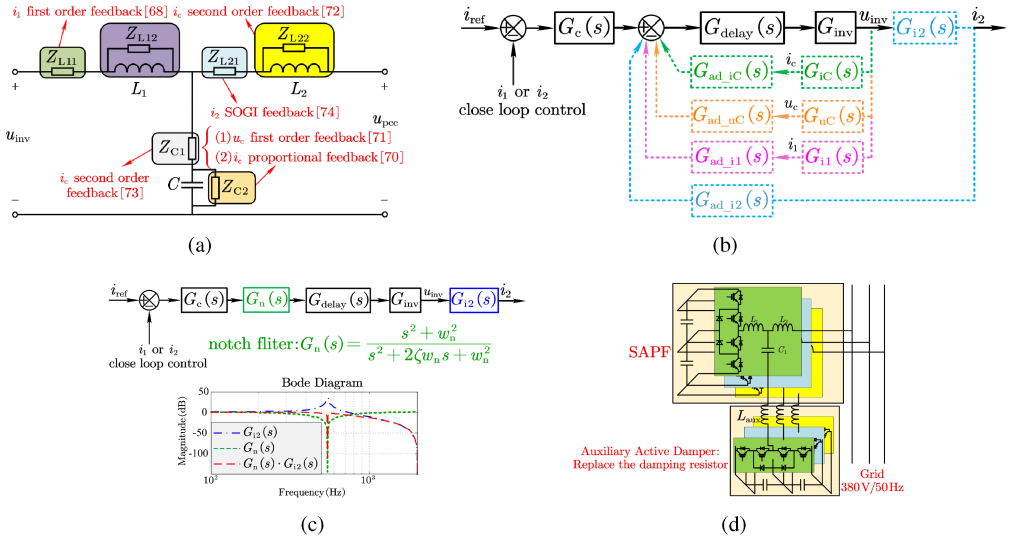

Fig. 4. Methods for changing inner impedance $Z_o(s)$. (a) PD. (b) AD based on state feedback. (c) Notch filter. (d) Auxiliary active damper.

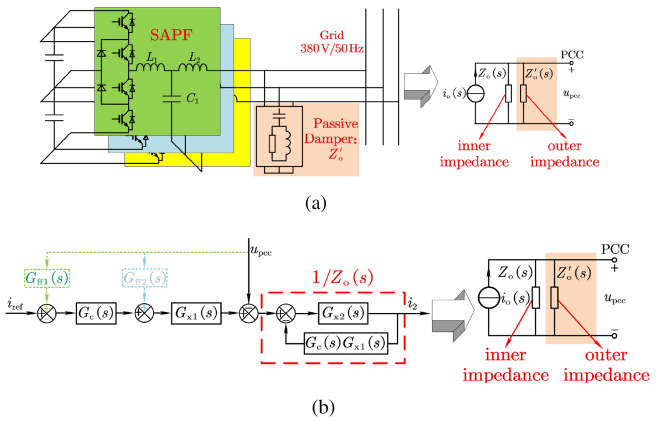

Fig. 5. Methods for changing outer impedance $Z'_o(s)$. (a) Passive dampers. (b) Voltage feedforward at the PCC.

TABLE II
COMPARISON OF DIFFERENT RESONANCE SUPPRESSION SCHEMES

Classification		Merit	Demerit
Inner impedance	PD	Simple and reliable	Resistance loss
	State feedback	1. No resistance loss 2. Flexible configuration of zeros and poles	1. Disable at high frequency 2. May require additional sensors
	Notch filter	No additional sensors required	1. Sensitive to parameter changes 2. Disable at high frequency
	Auxiliary circuit	Excellent damping effect	1. Complex structure 2. High cost
Outer impedance	Passive damper	Simple and reliable	Resistance loss
	Grid voltage feedforward	1. No resistance loss 2. Don't affect current control loop 3. No additional sensors	1. Disable at high frequency 2. May need harmonic detection

$$G_{iC}(s)=\frac{i_c(s)}{u_{\text{inv}}(s)}=\frac{1}{sL_1}\frac{s^2}{s^2+\omega_r^2} \tag{3}$$

$$G_{uC}(s)=\frac{u_c(s)}{u_{\text{inv}}(s)}=\frac{1}{L_1\,C}\frac{1}{s^2+\omega_r^2} \tag{4}$$

$$\omega_a=\sqrt{\frac{1}{L_2\,C}},\omega_r=\sqrt{\frac{L_1+L_2}{L_1L_2\,C}}. \tag{5}$$

In the low-frequency band, as shown in Fig. 4(a), the damping effect of AD based on state feedback is equivalent to that of PD. However, because the equivalent impedance of AD also accounts for the digital delay $G_{\text{delay}}(s)$ of digital control, its damping effect and robustness are lessened compared to PD [72], and a similar situation occurs when we adjust the outer virtual impedance. Then, as shown in Fig. 5, the parallel connection of passive dampers on the output side of SAPFs [73], [74] and the voltage feedforward at the point of common coupling (PCC) [75], [76] can be employed to modify the system's outer impedance so that the resonance phenomenon is inhibited. According to Yang et al. [76], the current control loop can be equivalently transformed to the Norton circuit in Fig. 5(b), where $G_c(s)$ is the transfer function of current controller, and $G_{x1}(s)$ and $G_{x2}(s)$ could be obtained from $G_c(s)$ and LCL filter. When we put PCC voltage at the output of current controller $G_c(s)$, the outer virtual impedance $Z'_o(s)$ introduced by the voltage feedforward can be expressed by (6) [76]. This method both reduces the interference of the grid voltage $u_g(s)$ on the output current $i_2(s)$ and increases system stability by configuring the outer virtual impedance to be of the same amplitude but opposite direction with inner impedance. Besides, the authors in [77], [78], and [79] use the harmonic detection or bandpass filter (BPF) to put on a partial information from the designated $u_{\text{pcc}}(s)$ frequency band at the same location as the reference current $i_{\text{ref}}(s)$, and the outer virtual impedance $Z'_o(s)$ introduced by the voltage feedforward can be expressed by (7). This technology provides positive damping for the specified band and lessens the detrimental impact of the negative impedance on system stability. Finally, Table II provides an assessment of the performance of different resonance suppression and impedance

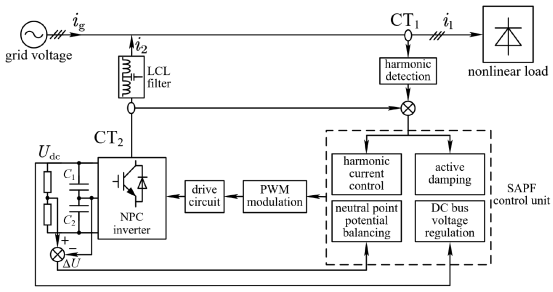

Fig. 6. Block diagram of the overall control strategy for a single SAPF.

reshaping strategies

$$Z_o'(s) = -\frac{1 + G_c G_{x1} G_{x2}}{G_{x2}\left(G_c G_{ff1} G_x - 1\right)} \tag{6}$$

$$Z_o'(s) = -\frac{1 + G_c G_{x1} G_{x2}}{G_{x2}\left(G_{ff2} G_x - 1\right)}. \tag{7}$$

C. Other Relevant Research Areas and a Block Diagram of the Overall Control Strategy for a Single SAPF

Along with the previously listed topics, it is also important to look into the methods of PWM, neutral point potential balancing for three-level SAPFs, and dc bus voltage regulation in the overall control strategy of a single SAPF. Last but not least, quick and effective current-limiting strategies are necessary because SAPF systems are susceptible to overcurrent phenomena when the nonlinear load on the system fluctuates significantly or in the case of a short circuit or breakage failure. Strategies such as truncated current-limiting control, proportional current-limiting control, and compound current limiting were proposed in [80] and [81], and they play a significant role in the safe functioning of APF systems. A block schematic of the entire control strategy for the single NPC three-level SAPF with the LCL filter is shown in Fig. 6. To accomplish effective grid harmonic correction, various control strategies must be organically combined.

III. Modeling and Stability Analysis of Multiparalleled SAPFs

Resonance issues between SAPFs, the grid impedance, and harmonic loads can jeopardize the safe and stable operation of the system when multiple SAPFs are connected in parallel to the grid. In Section III, we thoroughly examine the research on the modeling and stability analysis of multiparalleled SAPFs.

A. Circuit Model of Multiparalleled SAPF System

Without taking account of harmonic detection and harmonic load, two types of multiparalleled SAPF models were produced in Fig. 7 by extending at the PCC [82], [83]. It can be seen that each SAPF module is highly coupled with each other, and the output current $i_{2i(i=1,2,\ldots,N)}(s)$ of each SAPF contains three different excitation sources, which are from reference current of the local SAPF $i_{\text{refi}}(s)$, reference current of other SAPF $i_{\text{refj}}(s)$, and the grid voltage $u_g(s)$. The transfer function of output current $i_{2i}(s)$ of each SAPF module in Fig. 7(a) can be

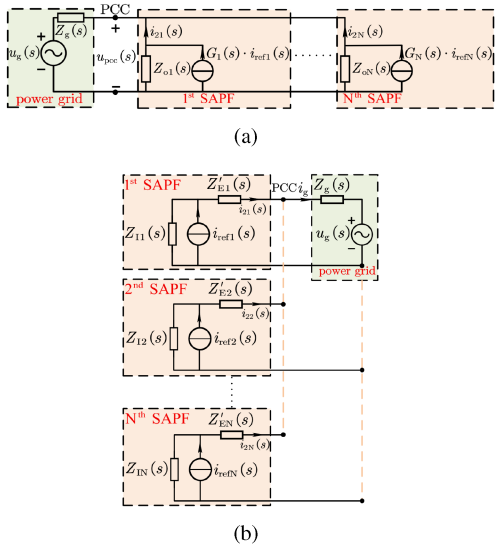

Fig. 7. Circuit models of multiparalleled SAPFs. (a) First Norton equivalent circuit. (b) Second Norton equivalent circuit.

obtained using Kirchhoff's law and the superposition theorem as (11) shown at the bottom of the next page, where $R_i(s)$, $R_{ij}(s)$, and $R_{ig}(s)$ represent transfer functions of these three excitation sources to $i_{2i}(s)$ [84]. Assuming that all the SAPF parameters are identical, each i_{refi} has the same impact on its own i_{2i}; the diagonal $R_i(s)$ is equal, i.e., $R_i(s) = R_1(s)$; nondiagonal $R_{ij}(i \neq j)$ is also equal since each i_{refi} has the same effect on the other i_{2j}, i.e., $R_{ij}(s) = R_{12}(s)$; obviously, $G_i(s)$ and $Z_{oi}(s)$ in each inverter are also exactly equal, i.e., $G_i(s) = G(s)$, $Z_{oi}(s) = Z_o(s)$. Therefore, we can get $R_i(s)$, $R_{ij}(s)$, and $R_{ig}(s)$ as

$$R_i(s) = \frac{(n-1)Z_g(s)G(s) + G(s)Z_o(s)}{nZ_g(s) + Z_o(s)} \tag{8}$$

$$R_{ij}(s) = \frac{(n-1)Z_g(s)G_o(s)}{nZ_g(s) + Z_o(s)} \tag{9}$$

$$R_{ig}(s) = 1/\left(nZ_g(s) + Z_o(s)\right). \tag{10}$$

According to the analysis of [17] and [85], assuming that the hardware and software parameters of all the SAPF modules and their command currents are the same, the equivalent grid impedance of any module in multiparalleled SAPFs increases to N times that when a single SAPF is connected to the power grid. Therefore, in this case, the equivalent Norton circuit of a single module in multiparalleled SAPFs can be obtained in Fig. 8. As the number of parallel modules N increases, the resonant frequency f_r between the grid impedance and LCL filters falls to within the control bandwidth, causing the system to become less stable [86]. The model proposed in references [87] and [88], which accounts for PWM harmonics and voltage feedforward at the Point of Common Coupling (PCC), highlights that the bode diagram of the closed-loop gain exhibits a higher resonance peak at higher frequency bands when the control and carrier signals are unsynchronized among multiple inverters, leading to decreased stability in the SAPF system. It is pointed out that the stability of SAPF system decreased, and the Bode

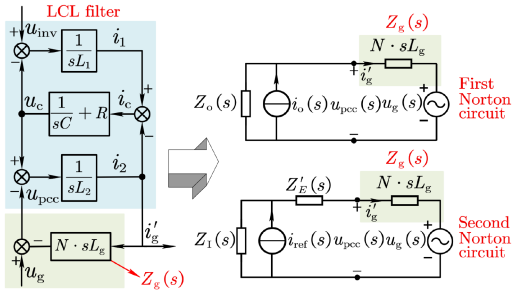

Fig. 8. Circuit model of a single SAPF in multiparalleled SAPFs, which have identical parameters.

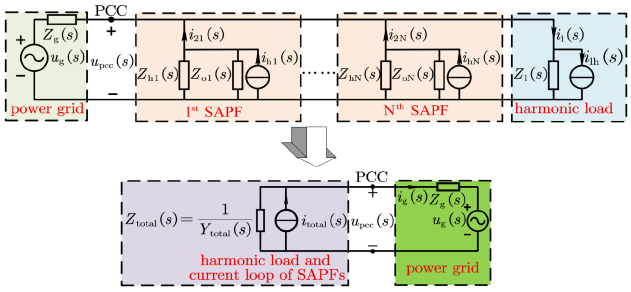

Fig. 9. Circuit model of multiparalleled SAPFs.

diagram of the closed-loop gain had a higher resonance peak at higher frequency bands when the control and carrier signals were not synchronized between multiple inverters. Then, the circuit model of multiparalleled SAPFs depicted in Fig. 9 was suggested by Liu et al. [77], which also took into account harmonic detection and harmonic load. Equation (12) is the resonant frequency between the LCL filter and the grid impedance in multiparalleled SAPFs, and (13) and (14) could be used to represent the overall response of grid current $i_g(s)$ and common coupling point voltage $u_{\text{pcc}}(s)$ [89], [90]

$$f_r = \frac{1}{2\pi}\sqrt{\frac{L_1 + L_2 + N \cdot L_g}{L_1\left(L_2 + N \cdot L_g\right)C_1}} \tag{12}$$

$$i_g(s) = \frac{i_{\text{total}}(s) - u_g(s)/Z_{\text{total}}(s)}{1 + Z_g(s)/Z_{\text{total}}(s)} \tag{13}$$

$$u_{\text{pcc}}(s) = \frac{u_g(s) + Z_g(s) \cdot i_{\text{total}}(s)}{1 + Z_g(s)/Z_{\text{total}}} . \tag{14}$$

To make the circuit model more realistic, in addition to the impact of the digital control delay and phase-locked loop [91], it is expected that the future research should focus on the model building of the nonlinear characteristics of power electronic converters, including PWM [92], dead-time effect [93], and nonideality of insulated-gate bipolar transistors or MOSFETs. Besides, the fractional-order technique may be used to more

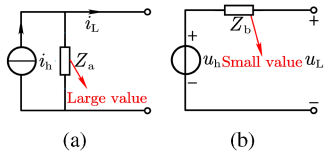

Fig. 10. Two different kinds of nonlinear load. (a) Current-source-type nonlinear load. (b) Voltage-source-type nonlinear load.

precisely describe the inductance and capacitance in the LCL filter [94], [95]. Apart from the current-source-type nonlinear load shown in Fig. 9, loads such as motor drives can be equivalent to a voltage source in series with a small resistance, as shown in Fig. 10. For the voltage-source type, the load impedance Z_b is relatively small, and the part of SAPF's output current flows into the load side, leading to an increase in load current, which is called the harmonic current amplification effect of voltage-source-type nonlinear load. It can be solved by connecting in series with a reactor or reducing the harmonic compensation rate [96], [97], [98]. Currently, modeling of harmonic loads only qualitatively distinguishes them as voltage- or current-source types, and a more thorough understanding is needed. In addition to the modeling ideas above, we can reduce the complexity of analysis by simplifying various parts of the system. For example, the complex harmonic detection $H(s)$ within the SAPF can be simplified as a BPF [99], $G(s)$ can be simplified as a low-pass filter [100], and the output resistance $Z_o(s)$ of the SAPF can be ignored, and the SAPF itself can be treated as a controlled current source [101].

B. Stability Analysis of Multiparalleled SAPFs

By the design guiding of a single SAPF in Section II, we can assume that each SAPF module is stable under an ideal grid, where $Z_g(s) = 0$. The essence of the stability analysis of the multiparalleled SAPF system covers the stability of all the responses, including PCC voltage u_{pcc}, output current $i_{2t}(t = 1, 2, \ldots, N)$ of each SAPF module, and total grid current i_g. The following subsection goes into the details of approaches available to analyze the stability of multiparalleled SAPFs, and we will draw attention to the impedance-based methods [102].

When using the PI controller or the low-order PR controller, we can ensure that the total impedance $Z_{\text{total}}(s)$ in Fig. 9 has only one intersection point f_i with the grid impedance $Z_g(s)$ in the amplitude–frequency characteristics of the bode diagram [103]. In this case, the idea of phase margin (PM) can be introduced, which must be positive and can be expressed as (15). As seen in Fig. 11, to improve stability robustness, it is also necessary to increase the phase of $Z_{\text{total}}(s)$ to acquire sufficient PM [76]

$$\text{PM} = 180^\circ - \left[\angle Z_g(f_i) - \angle Z_{\text{total}}(f_i)\right]. \tag{15}$$

$$\begin{bmatrix} i_{21}(s) \\ i_{22}(s) \\ \cdots \\ i_{2n}(s) \end{bmatrix} = \begin{bmatrix} R_1(s) & R_{12}(s) & \cdots & R_{1n}(s) \\ R_{21}(s) & R_2(s) & \cdots & R_{2n}(s) \\ \cdots & \cdots & \cdots & \cdots \\ R_{n1}(s) & R_{n2}(s) & \cdots & R_n(s) \end{bmatrix} \begin{bmatrix} i_{\text{ref1}}(s) \\ i_{\text{ref2}}(s) \\ \cdots \\ i_{\text{refn}}(s) \end{bmatrix} - \begin{bmatrix} R_{1g}(s) \\ R_{2g}(s) \\ \cdots \\ R_{ng}(s) \end{bmatrix} u_g(s). \tag{11}$$

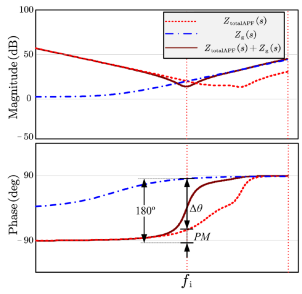

Fig. 11. Frequency responses of $Z_{\text{totalAPF}}(s)$, $Z_g(s)$, and the sum of the two impedances.

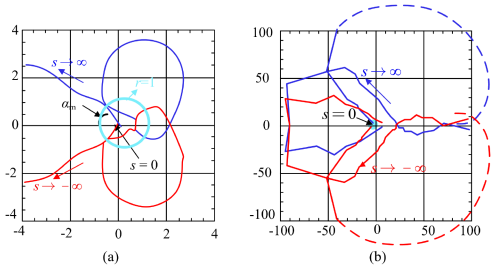

Fig. 12. Nyquist plot of $Z_g(s)/Z_{\text{total}}(s)$. (a) $R = 0$. (b) $R = 2$.

$Z_{\text{total}}(s)$ may cross $Z_g(s)$ more than once when an RC controller or a high-order PR controller is utilized, making it impossible to assess the system stability based on PM at this situation. To test if an inverter system is robust to grid impedance, Chen and Sun [90] and Sun [104] suggested examining whether the impedance ratio between the grid and SAPFs $Z_g(s)/Z_{\text{total}}(s)$ meets the Nyquist criteria. As seen in Fig. 12, if knowing the number of open-loop poles P and encirclements of the $(-1, 0)$ point R of $Z_g(s)/Z_{\text{total}}(s)$, we can determine whether the system is stable by whether (16) is equal to 0, where Z is the number of closed-loop poles [35]

$$Z = P - R. \tag{16}$$

It is feasible to analyze the closed-loop poles of a multiparalleled system in addition to using the approach of impedance ratio. According to [16] and [77], the total conductance $Y_{\text{total}}(s)$ in Fig. 9, which consists of the conductance of the grid $Y_g(s)$, the conductance of the harmonic load $Y_l(s)$, and the output conductance of the SAPF $Y_{hi}(s) + Y_{oi}(s), i \in (1, \ldots, N)$, determines whether the voltage response at the PCC is stable and, consequently, whether all the responses of the multiparalleled SAPF system are stable. Concretely, the right half-plane of $Y_{\text{GA}}(s)$ in s-domain having no zeros or its corresponding Nyquist diagram having zero number of encirclements around the origin is a sufficient and required condition for the multiparalleled system to be stable when a single module is stable. Besides, as illustrated in Fig. 13, we can divide the output current of each inverter module $i_{2i}(s)$ into common component i_{common} and interactive component $i_{\text{interactive\_}j}$ when disregarding the grid voltage, where $i_{\text{interactive\_}j}$ is the circulating current from the ith module to the jth module and i_{common} is the current injected to the grid; $i_{2i}(s)$ is given in (18), where $G_1(s)$ and $G_2(s)$ are the transfer functions of common current and interactive current to $i_{2i}(s)$. Then, we

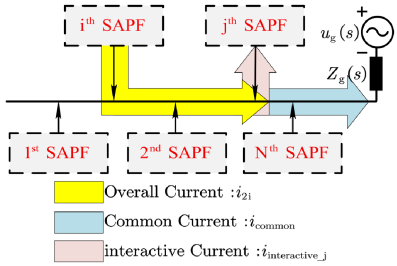

Fig. 13. Interactive current and common current in the multiparalleled system.

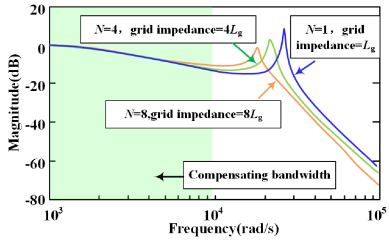

Fig. 14. Bode plot of $i'_g(s)/i_{\text{ref}}(s)$ in Fig. 8 when N is different.

can use the root-locus method to examine the stability of $G_1(s)$ and $G_2(s)$ under various parameters; if both $G_1(s)$ and $G_2(s)$ are stable, the system as a whole is stable [105], [106]

$$Y_{\text{total}}(s) = Y_g(s) + Y_l(s) + \sum_{i=1}^{N} Y_{hi}(s) + Y_{oi}(s) \tag{17}$$

$$i_{2i}(s) = G_1(s)\underbrace{(i_{\text{ref1}}(s) + \cdots + i_{\text{refN}}(s))}_{i_{\text{common}}(s)} + \sum_{j=1, j\neq i} G_2(s)\underbrace{(i_{\text{refi}}(s) - i_{\text{refj}}(s))}_{i_{\text{interactive\_}j}(s)}. \tag{18}$$

In general, the rated output current of a single SAPF is relatively high (usually between 50 and 200 A), and its corresponding total inverter-side inductance is between 100 and 300 μH. According to (12), when the SAPF adopts the LCL filter, its resonant frequency is usually between 5 and 15 kHz, often outside the compensating bandwidth (which is typically between 1.5 and 3 k) . When multiparalleled SAPFs have the same specification, Fig. 14 represents the closed-loop bode plot of the current loop $i'_g(s)/i_{\text{ref}}(s)$ of a certain SAPF module in the circuit model corresponding to Fig. 8. It can be observed that the frequency of resonance peak caused by the LCL filter shifts toward the compensating bandwidth. If this resonant frequency enters the compensating bandwidth, it would result in system instability. Specifically, considering only the excitation source of the first SAPF $i_{\text{ref1}}(s)$, transforming Fig. 7 yields Fig. 15. Fig. 15(a) shows the equivalent circuit diagram of multiple SAPFs operating in parallel, and the grid impedance, the equivalent impedance of the second SAPF, and the closed-loop bode plot of the current loop of the first SAPF are shown in Fig. 15(b). It can be seen that at the resonant frequency, the equivalent impedance of the second SAPF decreases sharply, far below the grid impedance, and the output current of the first SAPF flows into second rather than the grid, leading to the occurrence

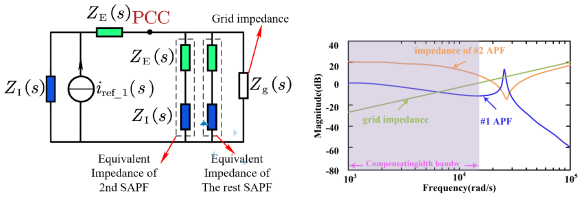

Fig. 15. Considering only the excitation source of the first SAPF $i_{\mathrm{ref1}}(s)$. (a) Equivalent circuit diagram of multiple SAPFs operating in parallel. (b) Bode plot of multiple SAPFs and grid impedance.

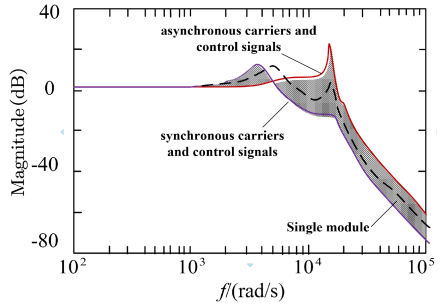

Fig. 16. Curve spectrum of output current frequency response excited by current reference $i_{21}(s)/i_{\mathrm{ref1}}(s)$.

of resonance phenomenon. The above discussion only considers the interaction between the grid impedance and multiple SAPFs, without considering the current sharing effect of harmonic loads.

When the system is connected to capacitive loads (such as voltage-source-type loads with capacitive characteristics) or when the current detection point includes reactive compensation capacitors, there is a risk of resonance instability in the system [99], [100]. We have reviewed resonance suppression techniques in the prior section. Similar to this, AD techniques based on state feedback [82], [83] are used to reduce the resonance peaks of LCL filters. In addition, virtual impedance techniques [77], [79] are employed to improve the robustness of multiparalleled systems in the weak grid. On the other hand, it is also possible to add global PD circuits or change the value of reactive power compensation capacitors. Then, as shown in Fig. 16, the resonance peak of the system increases, and its stability is reduced when the carriers and control signals are not synchronized between each module in the multiparalleled system [87], [88]. A hybrid system was created by combining two SAPF modules with different capacities, filter, and controller parameters. Subsequently, a corresponding parameter adjustment method was suggested [107]. It enables the system to achieve higher stability than a parallel connection of SAPFs with the same parameters.

In reality, the stability study of multiparalleled SAPFs has been a controversial topic until now. The stability assessments have been performed when using the current controller are PI, PR, and RC, but there is little information available of SMC, PC and composite controllers . Unresolved issues in the field are listed as follows:

1) simple and universal stability criteria for multiparalleled SAPFs with different specification parameters;

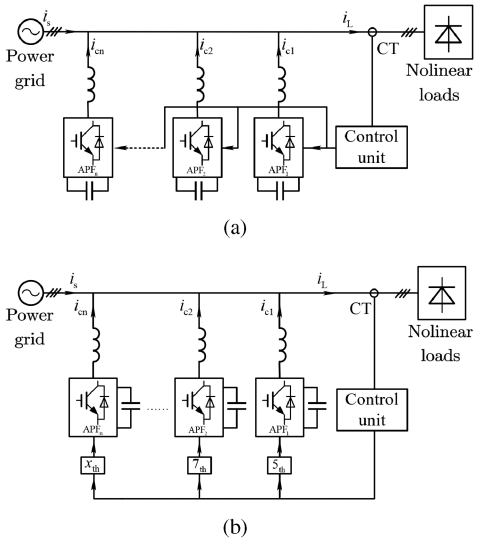

Fig. 17. Classifying by the compensation content. (a) In the capacity proportion mode. (b) In the frequency splitting mode.

2) stability analysis when working with other types of power quality regulators (e.g., reactive power compensation capacitors or static var generators);
3) how to assess multiparalleled system stability when using nonlinear control techniques such as SMC;
4) effect of output current limiting strategies of a single SAPF on the stability of multiparalleled SAPFs;
5) how to determine the specific parameters of the circuit model for different kinds of nonlinear loads;
6) how to dynamically suppress system resonances after online measurement of grid impedance, impedance of harmonic loads, and output impedance of SAPF module.

IV. Parallel Operation Strategies of Multiparalleled SAPFs

Numerous studies on the parallel operation strategies of multiparalleled SAPFs have been conducted, but they are dispersed and lack systematic summaries. In addition, its parallel operation has unique features when compared to conventional grid-connected inverters. In order to serve as a resource for upcoming researchers and engineering designers, the pros and cons of various operating techniques are examined from a variety of angles in this section.

A. Classifying Based on the Compensation Content of Each SAPF

In terms of compensation content, the parallel operation strategies of multiparalleled SAPFs can be divided into the capacity proportion mode and the frequency splitting mode [9], [10]. First, as depicted in Fig. 17(a), the parallel control unit assigns the output to each SAPF module based on its capacity, and in the event of a module failure, the controller can promptly adjust the command current in accordance with the remaining capacity of the modules, thereby facilitating scalability and being the prevalent approach in practical applications [86]. On

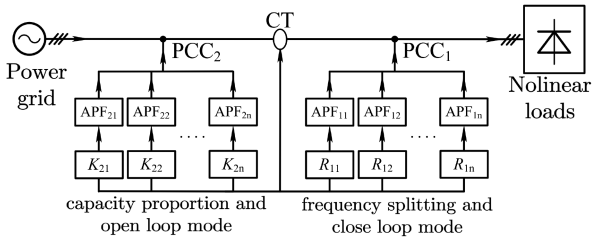

Fig. 18. Combination of open-loop control and closed-loop control.

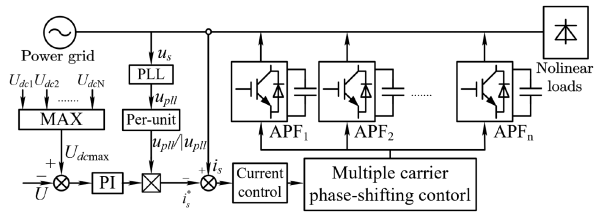

Fig. 19. Combination of DCC and CPS-SPWM.

the other hand, as shown in Fig. 17(b), the parallel control unit assigns the command current for each module based on different frequency bands. As per [108], the multiparalleled SAPF system with varying capacities is connected in parallel and divided according to its upper capacity limit, where the larger capacity compensates for the low-frequency harmonic components, and the smaller capacity compensates for the high-frequency harmonic components, thereby enhancing the utilization rate of SAPFs during operation. However, the frequency splitting mode necessitates the use of multiple SAPF specifications and prior knowledge of the site's harmonic data, hindering standardization and maintenance of the product. Furthermore, when one SAPF compensating a certain harmonic frequency band fails, a significant amount of harmonics in that band will enter the grid, undermining system reliability. Therefore, the frequency splitting mode is mainly employed in special circumstances, such as when the thermal performance of a capacity proportion mode cannot meet practical application requirements or the compensation effect is unsatisfactory, the frequency splitting mode can be considered as a solution to these issues.

B. Classification Based on the Location of CT

In the multiparalleled SAPF system, some researchers have combined open- and closed-loop control methods, as shown in Fig. 18, where multiple SAPFs are divided into two groups [16], [109]. The first group of SAPFs on the load side compensates harmonics with the frequency splitting mode and closed-loop control, using a lower switching frequency to compensate for low-frequency harmonics that have a higher content, with the frequency band of SAPF's output current being lower corresponding to a larger rated capacity, and closed-loop control can ensure the steady-state accuracy of the system. The second group of SAPFs on the grid side compensates harmonics with the capacity proportion mode and open-loop control, using a higher switching frequency to compensate for high-frequency harmonics that have a lower content, and open-loop control is used to ensure the dynamic performance of the system. This operating strategy implements the comprehensive optimization of compensation accuracy, capacity utilization, and dynamic response; nevertheless, the system structure is complex and requires many types of SAPF, which has a detrimental effect on reliability and mass production.

As shown in Fig. 19, a combination of DCC and carrier phase-shifted sinusoidal pulsewidth modulation (CPS-SPWM) for controlling parallel APFs was proposed in [110] and [111], which actually allocates compensation tasks proportionally to capacity. CPS-SPWM can be used to reduce the switching harmonic at the output of multiparalleled inverters and/or SAPFs, in which the carrier phase of each SAPF is delayed by $2\pi/N$ sequentially when the number of modules is N, thereby improving the equivalent switching frequency of the system's output compensation current. However, this method requires high real-time control requirements, and carrier asynchrony will not only reduce system stability but also result in circulating currents between modules [112]. This operating strategy can greatly simplify the hardware and control system design of the system and is relatively accurate due to the use of closed-loop control, although the system's dynamic response time is slightly slower compared to other open-loop control schemes, and the dc-side voltage fluctuates greatly when the system's harmonic load changes, resulting in poor system stability [31].

C. Classification Based on the Type of Leader Controller

The parallel operation strategies of multiparalleled SAPFs can be classified into three categories based on the leader controller: centralized control, leader–follower control [113], [114], and decentralized control [115].

In centralized control, a single leader controller transmits the allocated capacity and frequency information to multiple SAPFs. Harmonic sampling and extraction can be accomplished either by the leader controller or by each SAPF independently. This system has a relatively low cost and is simple to implement, which results in good real-time performance, making it the most widely used method for controlling the multimodule system. However, it is also highly influenced by the leader controller. In the leader–follower control, one SAPF is designated as the leader, while the rest are followers. The leader acts as the central controller and dictates the actions of the followers. In the leader–follower control method, one SAPF is designated as the leader, while the rest are followers. The leader acts as the central controller and dictates the actions of the followers. In the event of a failure of the leader, the other followers can select a new leader through a competition mechanism, thus overcoming the drawbacks of centralized control.

In distributed control, there exists no leader controller, and each module is equal in status, containing a current-sharing control unit. The modules operate in parallel through simple communication and/or droop characteristics [116], [117]. In addition, multiple SAPFs can be sorted by distance to harmonic loads. The closer to the harmonic sources, the more compensation; the farther away, the less compensation as a redundant

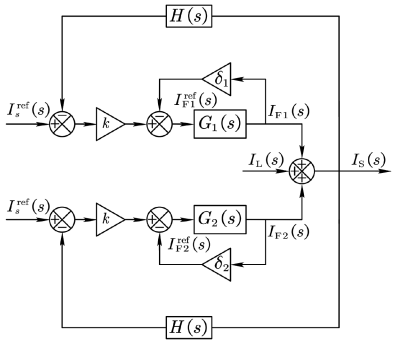

Fig. 20. Simplified control block diagram of the droop-control system comprising two SAPF modules.

unit [116]. As shown in Fig. 20, a parallel operation strategy for two SAPFs that employs a distributed control with droop characteristics $\delta_i (i = 1, 2)$ was presented in [117], where k is the gain of grid harmonic current, $H(s)$ is a notch filter used to filter out the fundamental harmonic current from the grid, $G_i(s)$ represents the closed-loop transfer function of the current loop for the ith SAPF, I_S is the grid current, I_F is the output current of SAPF, I_L is the current of harmonic load, and I_S^{ref} is the reference grid current that is usually set as zero. The approximate transfer function of the current loop of the ith SAPF module is shown in (19). Combining it with Fig. 20, the output current of the two modules at lower frequencies can be expressed as (20). From (20), it can be inferred that the current sharing between SAPF modules is a function of the corresponding droop coefficient. However, the study on the droop coefficient is currently at a qualitative stage, and a quantitative method for droop coefficients has not yet been thoroughly studied. In addition, the compensation precision is relatively low due to the general softening of outer characteristics in droop control

$$G_i(s) = \frac{\omega_{ci}}{s + \omega_{ci}} \tag{19}$$

$$\left|\frac{I_{F1}}{I_{F2}}\right| = \lim_{s\to 0}\left|\left(\frac{s+\omega_{c1}}{s+\omega_{c2}}\right)\left(\frac{s+\omega_{c2}+\delta_2\omega_{c2}}{s+\omega_{c1}+\delta_1\omega_{c1}}\right)\right| = \frac{1+\delta_2}{1+\delta_1}. \tag{20}$$

D. Fault-Tolerant Control Within a Module and Between Multiple Modules

For multiparalleled SAPFs, it is desirable to have fewer modules in service while ensuring sufficient compensation for nonlinear harmonics. This leaves more redundant SAPFs to ensure system reliability with lower switching loss and higher efficiency. With the premise of redundancy, fault-tolerant control can be performed between a single SAPF module and multiple SAPF modules.

Fig. 21(a) shows the fault-tolerant control technology for a single SAPF module. When a bridge arm fails, the inverter can be changed to a three-phase four-switch topology by changing the dc midpoint position and adjusting the corresponding modulation mode, so that the module can still work normally [118]. Fig. 21(b) shows the fault-tolerant control technology of multiparalleled SAPFs. Two SAPF modules are paralleled and both

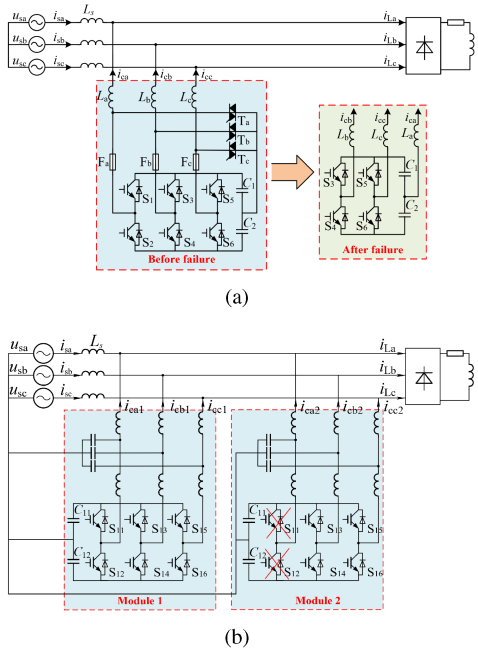

Fig. 21. Structure of fault-tolerant control. (a) Single module. (b) Multiple modules.

compensate according to their capacity ratios. When the second SAPF module's a-phase fails, the a-phase bridge arm of the second module is blocked and its current sharing coefficient is allocated to the first module, meaning that the first module's a-phase takes over the task of the second module's a-phase. For SAPF systems with more modules, the method is similar: first, cut off the faulty module's faulty phase, then distribute its compensation tasks evenly among the other modules, and the other two phases of the faulty module continue to work normally [119], [120].

In conclusion, this method improves the reliability of the system, and the system can still operate normally under fault conditions. However, it has a relatively complex algorithm that must be combined with fault diagnosis technology and requires the system to have some redundant capacity. Therefore, it is rarely used in engineering applications now.

E. Comprehensive Comparative Analysis of Various Parallel Operation Strategies

Currently, there is no parallel operation strategy of multiparalleled SAPFs that can be applied to all situations, and comparative research on the performance of various operation strategies has been conducted. This makes it difficult to objectively compare the advantages and disadvantages of various parallel operation strategies under different application conditions. As shown in Table III, this subsection summarizes the common parallel operation strategies and summarizes their advantages and disadvantages. For multiparalleled SAPFs, the current mainstream method is centralized control + capacity proportion mode, while the frequency splitting mode and other strategies are applied to some special situations according to actual engineering needs.

TABLE III
MERITS AND DEMERITS OF DIFFERENT PARALLEL OPERATION STRATEGIES

Parallel operation strategies	Merits	Demerits
Centralized control and capacity proportion mode	1. The algorithm is simple. 2. It has strong scalability. 3. The technology is mature and widely used.	The impact of the leader controller is too significant.
Frequency splitting mode	1. High capacity utilization. 2. The algorithm is simple	1. Relatively poor reliability. 2. Requires modules with different specifications 3. Requires known and relatively certain harmonic data
Leader-follower control	High reliability	The switchover between the Leader and slaves may fail
Distributed control and/or droop control	1. Simple and reliable. 2. Low interference between modules.	Low compensation accuracy
Fault-tolerant control	The system has high reliability and can continue operating during a fault.	1. Complex control algorithm. 2. Need to combine with fault diagnosis technology.
Direct current control (DCC)	1. Simple hardware structure. 2. High steady-state accuracy	Slow dynamic response.
Combination of open-loop control and closed-loop control	Simultaneously balancing the steady-state accuracy and dynamic performance.	1. High cost. 2. Complex system structure, unfavorable for large-scale production.
CPS-SPWM	Suppressing switch ripples.	1. High control accuracy requirement. 2. Poor stability. 3. Circulation current between modules

V. CONCLUSION AND FUTURE WORK

With the advancement of power electronic power systems, power quality issues have become widespread in various situations. To address these issues, high-capacity APFs are increasingly being utilized to improve power system quality. We present a classification and summary of multiparalleled SAPFs and provide detailed descriptions of the modeling and stability analysis, control strategies of a single SAPF, and parallel operation strategies. Finally, the future research trends of multiparalleled SAPFs can be summarized as follows.

1) Multiparalleled SAPFs are the primary methods for compensating large-capacity harmonic and reactive, thanks to their advantages of easy capacity expansion, simple maintenance, and reliable operation.
2) Research on the topology of a single SAPF module is very mature, with the main configuration being a diode-clamped inverter + LCL filter. Therefore, the research focuses on the harmonic detection techniques, harmonic current control techniques, and resonance suppression techniques of a single SAPF module. Currently, the mainstream control algorithm in industrial applications involves ip-iq/DFT/FFT harmonic detection with PR/RC harmonic current control. Advanced intelligent control algorithms are limited by the complexity of their implementation and are typically validated for their effectiveness through simulation or semiphysical simulation platforms like dSPACE. In the future, if we aim to implement advanced intelligent control algorithms on a large scale, we can enhance the computational power of digital controllers through hardware improvements. In addition, it is feasible to simplify the intelligent control algorithms in a reasonable manner.
3) One unresolved issue in the modeling of multiparalleled SAPFs is the inability to accurately represent harmonic loads, such as diode rectifier bridges using transfer functions in the s-domain or z-domain. Therefore, it is difficult to consider the influence of harmonic loads in stability analysis. However, in reality, if the capacitance value of the dc-side filter capacitor of the diode rectifier bridge is large and the inductance value of the input or output reactance is small, it may lead to system instability and harmonic current amplification effect. Describing this problem using appropriate mathematical language remains an unresolved issue.
4) The mainstream parallel operation strategy of multiparalleled SAPFs in industrial applications is centralized control and capacity proportion mode. However, this may not meet all engineering requirements. Engineers and researchers have proposed a series of solutions to improve the stability and reliability of multiparalleled SAPFs and reduce the implementation difficulty. Currently, there are no quantitative data available to compare the performance of different schemes. We offer a qualitative comparison of the benefits and drawbacks of various solution types, with the goal of offering practical guidance for engineering applications.

REFERENCES

[1] B. Bird, J. Marsh, and P. McLellan, "Harmonic reduction in multiplex convertors by triple-frequency current injection," in *Proc. Inst. Elect. Eng.*, 1969, pp. 1730–1734.
[2] Z. Wang, Q. Wang, W. Yao, and J. Liu, "A series active power filter adopting hybrid control approach," *IEEE Trans. Power Electron.*, vol. 16, no. 3, pp. 301–310, May 2001.
[3] J. W. Dixon, G. Venegas, and L. A. Moran, "A series active power filter based on a sinusoidal current-controlled voltage-source inverter," *IEEE Trans. Ind. Electron.*, vol. 44, no. 5, pp. 612–620, Oct. 1997.
[4] V. Khadkikar, "Enhancing electric power quality using UPQC: A comprehensive overview," *IEEE Trans. Power Electron.*, vol. 27, no. 5, pp. 2284–2297, May 2012.

[5] W. U. Tareen, S. Mekhilef, M. Seyedmahmoudian, and B. Horan, "Active power filter (APF) for mitigation of power quality issues in grid integration of wind and photovoltaic energy conversion system," *Renewable Sustain. Energy Rev.*, vol. 70, pp. 635–655, 2017.

[6] D. Li, T. Wang, W. Pan, X. Ding, and J. Gong, "A comprehensive review of improving power quality using active power filters," *Electr. Power Syst. Res.*, vol. 199, 2021, Art. no. 107389.

[7] A. M. Massoud, S. J. Finney, and B. W. Williams, "Review of harmonic current extraction techniques for an active power filter," in *Proc. 11th Int. Conf. Harmon. Qual. Power*, 2004, pp. 154–159.

[8] Y. Hoon, M. A. Mohd Radzi, M. K. Hassan, and N. F. Mailah, "Control algorithms of shunt active power filter for harmonics mitigation: A review," *Energies*, vol. 10, no. 12, 2017, Art. no. 2038.

[9] S. K. Khadem, M. Basu, and M. F. Conlon, "A review of parallel operation of active power filters in the distributed generation system," in *Proc. Eur. Conf. Power Electron. Appl.*, 2011, pp. 1–10.

[10] S. K. Khadem, M. Basu, and M. F. Conlon, "Parallel operation of inverters and active power filters in distributed generation system—A review," *Renewable Sustain. Energy Rev.*, vol. 15, no. 9, pp. 5155–5168, 2011.

[11] W.-H. Choi, C.-S. Lam, M.-C. Wong, and Y.-D. Han, "Analysis of dc-link voltage controls in three-phase four-wire hybrid active power filters," *IEEE Trans. Power Electron.*, vol. 28, no. 5, pp. 2180–2191, May 2013.

[12] A. Bhattacharya, C. Chakraborty, and S. Bhattacharya, "Parallel-connected shunt hybrid active power filters operating at different switching frequencies for improved performance," *IEEE Trans. Ind. Electron.*, vol. 59, no. 11, pp. 4007–4019, Nov. 2012.

[13] F. T. Ghetti, A. A. Ferreira, H. A. Braga, and P. G. Barbosa, "A study of shunt active power filter based on modular multilevel converter (MMC)," in *Proc. IEEE/IAS 10th Int. Conf. Ind. Appl.*, 2012, pp. 1–6.

[14] Z. Shu, M. Liu, L. Zhao, S. Song, Q. Zhou, and X. He, "Predictive harmonic control and its optimal digital implementation for MMC-based active power filter," *IEEE Trans. Ind. Electron.*, vol. 63, no. 8, pp. 5244–5254, Aug. 2016.

[15] F. Zhuo, H. Li, H. Li, and Z. Wang, "Main circuit consist of multiplex use for active power filter," in *Proc. Int. Conf. Elect. Mach. Syst.*, 2001, pp. 504–507.

[16] K. Liu, W. Cao, and J. Zhao, "Dual-loop-based harmonic current control strategy and admittance modeling for a multimodular parallel SAPFs system," *IEEE Trans. Ind. Electron.*, vol. 67, no. 7, pp. 5456–5466, Jul. 2020.

[17] Y. Wang, J. Xu, L. Feng, and C. Wang, "A novel hybrid modular three-level shunt active power filter," *IEEE Trans. Power Electron.*, vol. 33, no. 9, pp. 7591–7600, Sep. 2018.

[18] L. S. Czarnecki, "On some misinterpretations of the instantaneous reactive power P-Q theory," *IEEE Trans. Power Electron.*, vol. 19, no. 3, pp. 828–836, May 2004.

[19] R. S. Herrera, P. Salmerón, and H. Kim, "Instantaneous reactive power theory applied to active power filter compensation: Different approaches, assessment, and experimental results," *IEEE Trans. Ind. Electron.*, vol. 55, no. 1, pp. 184–196, Jan. 2008.

[20] K. Zhou, A. Luo, X. Xia, and W. Zhao, "An improved ip-iq harmonic current detecting method and digital low-pass filter's optimized design," *Proc. CSEE*, vol. 27, no. 34, pp. 96–101, 2007.

[21] H. Wen, Z. Teng, and S. Guo, "Triangular self-convolution window with desirable sidelobe behaviors for harmonic analysis of power system," *IEEE Trans. Instrum. Meas.*, vol. 59, no. 3, pp. 543–552, Mar. 2010.

[22] A. V. Oppenheim, *Discrete-Time Signal Processing*. Noida, India: Pearson Education India, 1999.

[23] S. Srianthumrong and S. Sangwongwanich, "An active power filter with harmonic detection method based on recursive DFT," in *Proc. 8th Int. Conf. Harmon. Qual. Power. Process.*, 1998, pp. 127–132.

[24] T. Grandke, "Interpolation algorithms for discrete fourier transforms of weighted signals," *IEEE Trans. Instrum. Meas.*, vol. IM-32, no. 2, pp. 350–355, Jun. 1983.

[25] G. Andria, M. Savino, and A. Trotta, "Windows and interpolation algorithms to improve electrical measurement accuracy," *IEEE Trans. Instrum. Meas.*, vol. 38, no. 4, pp. 856–863, Aug. 1989.

[26] X. Guo, W. Wu, and Z. Chen, "Multiple-complex coefficient-filter-based phase-locked loop and synchronization technique for three-phase grid-interfaced converters in distributed utility networks," *IEEE Trans. Ind. Electron.*, vol. 58, no. 4, pp. 1194–1204, Apr. 2011.

[27] F. Costa, A. Cardoso, and D. A. Fernandes, "Harmonic analysis based on Kalman filtering and Prony's method," in *Proc. Int. Conf. Power Eng., Energy Elect. Drives*, 2007, pp. 696–701.

[28] V. Pham and K. Wong, "Wavelet-transform-based algorithm for harmonic analysis of power system waveforms," *Proc. Inst. Elect. Eng.—Gener., Transmiss. Distrib.*, vol. 146, no. 3, pp. 249–254, 1999.

[29] H. Akagi, A. Nabae, and S. Atoh, "Control strategy of active power filters using multiple voltage-source PWM converters," *IEEE Trans. Ind. Appl.*, vol. IA-22, no. 3, pp. 460–465, May 1986.

[30] P. Mattavelli, "A closed-loop selective harmonic compensation for active filters," *IEEE Trans. Ind. Appl.*, vol. 37, no. 1, pp. 81–89, Jan./Feb. 2001.

[31] Q.-N. Trinh and H.-H. Lee, "An advanced current control strategy for three-phase shunt active power filters," *IEEE Trans. Ind. Electron.*, vol. 60, no. 12, pp. 5400–5410, Dec. 2013.

[32] W. Zhaoan, *Harmonic Suppression and Reactive Power Compensation*. Beijing, China: China Machine Press, 2016.

[33] X. Sun, J. Zeng, N. Li, and X. Li, "Improvement for the closed-loop control of shunt active power filter based on feedback of supply-side current," *Trans. China Electrotech. Soc.*, vol. 27, no. 10, pp. 150–154, 2012.

[34] W. Guang-Zhu, "Equivalence principle of current control for shunt active power filters," *Proc. CSEE*, vol. 26, no. 15, p. 6, 2006.

[35] G. F. Franklin, J. D. Powell, A. Emami-Naeini, and J. D. Powell, *Feedback Control of Dynamic Systems*, vol. 4. Hoboken, NJ, USA: Prentice-Hall, 2002 .

[36] R. Griñó, R. Cardoner, R. Costa-Castelló, and E. Fossas, "Digital repetitive control of a three-phase four-wire shunt active filter," *IEEE Trans. Ind. Electron.*, vol. 54, no. 3, pp. 1495–1503, Jun. 2007.

[37] Z. Zeng, J.-Q. Yang, S.-L. Chen, and J. Huang, "Fast-transient repetitive control strategy for a three-phase LCL filter-based shunt active power filter," *J. Power Electron.*, vol. 14, no. 2, pp. 392–401, 2014.

[38] L. Herman, I. Papic, and B. Blazic, "A proportional-resonant current controller for selective harmonic compensation in a hybrid active power filter," *IEEE Trans. Power Del.*, vol. 29, no. 5, pp. 2055–2065, Oct. 2014.

[39] A. Vidal et al., "Assessment and optimization of the transient response of proportional-resonant current controllers for distributed power generation systems," *IEEE Trans. Ind. Electron.*, vol. 60, no. 4, pp. 1367–1383, Apr. 2013.

[40] C. Lascu, L. Asiminoaei, I. Boldea, and F. Blaabjerg, "Frequency response analysis of current controllers for selective harmonic compensation in active power filters," *IEEE Trans. Ind. Electron.*, vol. 56, no. 2, pp. 337–347, Feb. 2009.

[41] B. A. Francis and W. M. Wonham, "The internal model principle for linear multivariable regulators," *Appl. Math. Optim.*, vol. 2, no. 2, pp. 170–194, 1975.

[42] B. A. Francis and W. M. Wonham, "The internal model principle of control theory," *Automatica*, vol. 12, no. 5, pp. 457–465, 1976.

[43] W. Jiang, X. Ding, Y. Ni, J. Wang, W. Lei, and W. Ma, "An improved deadbeat control for a three-phase three-line active power filter with current-tracking error compensation," *IEEE Trans. Power Electron.*, vol. 33, no. 3, pp. 2061–2072, Mar. 2018.

[44] M. Odavic, V. Biagini, P. Zanchetta, M. Sumner, and M. Degano, "One-sample-period-ahead predictive current control for high-performance active shunt power filters," *IET Power Electron.*, vol. 4, no. 4, pp. 414–423, 2011.

[45] C. Gong, W.-K. Sou, and C.-S. Lam, "Second-order sliding-mode current controller for LC-coupling hybrid active power filter," *IEEE Trans. Ind. Electron.*, vol. 68, no. 3, pp. 1883–1894, Mar. 2021.

[46] J. Fei and Y. Chen, "Dynamic terminal sliding-mode control for single-phase active power filter using new feedback recurrent neural network," *IEEE Trans. Power Electron.*, vol. 35, no. 9, pp. 9904–9922, Sep. 2020.

[47] P. Acuna, L. Morán, M. Rivera, R. Aguilera, R. Burgos, and V. G. Agelidis, "A single-objective predictive control method for a multivariable single-phase three-level NPC converter-based active power filter," *IEEE Trans. Ind. Electron.*, vol. 62, no. 7, pp. 4598–4607, Jul. 2015.

[48] L. Tarisciotti et al., "Model predictive control for shunt active filters with fixed switching frequency," *IEEE Trans. Ind. Appl.*, vol. 53, no. 1, pp. 296–304, Jan./Feb. 2016.

[49] Y. Liang, J. Liu, and Z. Li, "Improved deadbeat-repetitive control strategy for active power filter," *Trans. China Electrotech. Soc.*, vol. 33, no. 19, p. 10, 2018.

[50] L. Shi, R. Cai, L. Chen, and P. Wang, "A deadbeat control scheme for three-phase three-wire active power filter," *Power Syst. Protection Control*, vol. 42, no. 14, pp. 32–37, 2014.

[51] Y. Fang, J. Fei, and D. Cao, "Adaptive fuzzy-neural fractional-order current control of active power filter with finite-time sliding controller," *Int. J. Fuzzy Syst.*, vol. 21, no. 5, pp. 1533–1543, 2019.

[52] A. K. Mishra, S. R. Das, P. K. Ray, R. K. Mallick, and D. K. Mishra, "PSO-GWO optimized fractional order PID based hybrid shunt active power filter for power quality improvements," *IEEE Access*, vol. 8, pp. 74497–74512, 2020.

[53] N. Liu and J. Fei, "Adaptive fractional sliding mode control of active power filter based on dual RBF neural networks," *IEEE Access*, vol. 5, pp. 27590–27598, 2017.

[54] S. Hou, Y. Chu, and J. Fei, "Intelligent global sliding mode control using recurrent feature selection neural network for active power filter," *IEEE Trans. Ind. Electron.*, vol. 68, no. 8, pp. 7320–7329, Aug. 2021.

[55] J. Fei, H. Wang, and Y. Fang, "Novel neural network fractional-order sliding-mode control with application to active power filter," *IEEE Trans. Syst., Man, Cybern. Syst.*, vol. 52, no. 6, pp. 3508–3518, Jun. 2022.

[56] R. Teodorescu, F. Blaabjerg, M. Liserre, and A. Dell'Aquila, "A stable three-phase LCL-filter based active rectifier without damping," in *Proc. 38th IAS Annu. Meeting Conf. Rec. Ind. Appl. Conf.*, 2003, pp. 1552–1557.

[57] J. Dannehl, C. Wessels, and F. W. Fuchs, "Limitations of voltage-oriented PI current control of grid-connected PWM rectifiers with LCL filters," *IEEE Trans. Ind. Electron.*, vol. 56, no. 2, pp. 380–388, Feb. 2009.

[58] R. Pena-Alzola, M. Liserre, F. Blaabjerg, R. Sebastián, J. Dannehl, and F. W. Fuchs, "Analysis of the passive damping losses in LCL-filter-based grid converters," *IEEE Trans. Power Electron.*, vol. 28, no. 6, pp. 2642–2646, Jun. 2013.

[59] R. N. Beres, X. Wang, F. Blaabjerg, M. Liserre, and C. L. Bak, "Optimal design of high-order passive-damped filters for grid-connected applications," *IEEE Trans. Power Electron.*, vol. 31, no. 3, pp. 2083–2098, Mar. 2016.

[60] Y. Han et al., "Modeling and stability analysis of LCL-type grid-connected inverters: A comprehensive overview," *IEEE Access*, vol. 7, pp. 114975–115001, 2019.

[61] C. C. Gomes, A. F. Cupertino, and H. A. Pereira, "Damping techniques for grid-connected voltage source converters based on LCL filter: An overview," *Renewable Sustain. Energy Rev.*, vol. 81, pp. 116–135, 2018.

[62] Y. Guan, Y. Wang, Y. Xie, Y. Liang, A. Lin, and X. Wang, "The dual-current control strategy of grid-connected inverter with LCL filter," *IEEE Trans. Power Electron.*, vol. 34, no. 6, pp. 5940–5952, Jun. 2019.

[63] X. Wang, F. Blaabjerg, and P. C. Loh, "Grid-current-feedback active damping for LCL resonance in grid-connected voltage-source converters," *IEEE Trans. Power Electron.*, vol. 31, no. 1, pp. 213–223, Jan. 2016.

[64] T. Gao, Y. Lin, D. Chen, and L. Xiao, "A novel active damping control based on grid-side current feedback for LCL-filter active power filter," *Energy Rep.*, vol. 6, pp. 1318–1324, 2020.

[65] X. Zhou et al., "Robust grid-current-feedback resonance suppression method for LCL-type grid-connected inverter connected to weak grid," *IEEE Trans. Emerg. Sel. Topics Power Electron.*, vol. 6, no. 4, pp. 2126–2137, Dec. 2018.

[66] S. G. Parker, B. P. McGrath, and D. G. Holmes, "Regions of active damping control for LCL filters," *IEEE Trans. Ind. Appl.*, vol. 50, no. 1, pp. 424–432, Jan./Feb. 2014.

[67] H.-C. Chen, P.-T. Cheng, X. Wang, and F. Blaabjerg, "A passivity-based stability analysis of the active damping technique in the offshore wind farm applications," *IEEE Trans. Ind. Appl.*, vol. 54, no. 5, pp. 5074–5082, Sep./Oct. 2018.

[68] J. Dannehl, F. W. Fuchs, S. Hansen, and P. B. Thøgersen, "Investigation of active damping approaches for PI-based current control of grid-connected pulse width modulation converters with LCL filters," *IEEE Trans. Ind. Appl.*, vol. 46, no. 4, pp. 1509–1517, Jul./Aug. 2010.

[69] M. Büyük, A. Tan, and M. Tümay, "Improved adaptive notch filter-based active damping method for shunt active power filter with LCL-filter," *Elect. Eng.*, vol. 100, no. 3, pp. 2037–2049, 2018.

[70] E. Rodriguez-Diaz, F. D. Freijedo, J. C. Vasquez, and J. M. Guerrero, "Analysis and comparison of notch filter and capacitor voltage feedforward active damping techniques for LCL grid-connected converters," *IEEE Trans. Power Electron.*, vol. 34, no. 4, pp. 3958–3972, Apr. 2019.

[71] M. Büyük, A. Tan, and M. Tümay, "Resonance suppression of LCL filter for shunt active power filter via active damper," *Int. J. Elect. Power Energy Syst.*, vol. 134, 2022, Art. no. 107389.

[72] L. Yang and J. Yang, "A robust dual-loop current control method with a delay-compensation control link for LCL-type shunt active power filters," *IEEE Trans. Power Electron.*, vol. 34, no. 7, pp. 6183–6199, Jul. 2019.

[73] Z. Salam, P. C. Tan, and A. Jusoh, "Harmonics mitigation using active power filter: A technological review," *Elektrika J. Elect. Eng.*, vol. 8, no. 2, pp. 17–26, 2006.

[74] Y. Xu, X. Xiao, H. Liu, and H. Wang, "Parallel operation of hybrid active power filter with passive power filter or capacitors," in *Proc. IEEE/PES Transmiss. Distrib. Conf. Expo.: Asia Pacific*, 2005, pp. 1–6.

[75] X. Wang, Y. W. Li, F. Blaabjerg, and P. C. Loh, "Virtual-impedance-based control for voltage-source and current-source converters," *IEEE Trans. Power Electron.*, vol. 30, no. 12, pp. 7019–7037, Dec. 2015.

[76] D. Yang, X. Ruan, and H. Wu, "Impedance shaping of the grid-connected inverter with LCL filter to improve its adaptability to the weak grid condition," *IEEE Trans. Power Electron.*, vol. 29, no. 11, pp. 5795–5805, Nov. 2014.

[77] K. Liu et al., "Admittance modeling, analysis, and reshaping of harmonic control loop for multiparalleled SAPFs system," *IEEE Trans. Ind. Inform.*, vol. 17, no. 1, pp. 280–289, Jan. 2021 .

[78] K. M. Alawasa, Y. A.-R. I. Mohamed, and W. Xu, "Active mitigation of subsynchronous interactions between PWM voltage-source converters and power networks," *IEEE Trans. Power Electron.*, vol. 29, no. 1, pp. 121–134, Jan. 2014.

[79] X. Wang, F. Blaabjerg, M. Liserre, Z. Chen, J. He, and Y. Li, "An active damper for stabilizing power-electronics-based ac systems," *IEEE Trans. Power Electron.*, vol. 29, no. 7, pp. 3318–3329, Jul. 2014.

[80] S. Chiang and J. Chang, "Parallel operation of shunt active power filters with capacity limitation control," *IEEE Trans. Aerosp. Electron. Syst.*, vol. 37, no. 4, pp. 1312–1320, Oct. 2001.

[81] W. Cao, M. Wu, J. Zhao, W. Liu, and Y. Lu, "An improved current-limiting strategy for shunt active power filter (SAPF) using particle swarm optimization (PSO)," in *Proc. IEEE Appl. Power Electron. Conf. Expo.*, 2018, pp. 494–498.

[82] L. Feng and Y. Wang, "Modeling and resonance control of modular three-level shunt active power filter," *IEEE Trans. Ind. Electron.*, vol. 64, no. 9, pp. 7478–7486, Sep. 2017.

[83] J. He, Y. W. Li, D. Bosnjak, and B. Harris, "Investigation and active damping of multiple resonances in a parallel-inverter-based microgrid," *IEEE Trans. Power Electron.*, vol. 28, no. 1, pp. 234–246, Jan. 2013.

[84] M. Lu, Y. Yang, B. Johnson, and F. Blaabjerg, "An interaction-admittance model for multi-inverter grid-connected systems," *IEEE Trans. Power Electron.*, vol. 34, no. 8, pp. 7542–7557, Aug. 2019.

[85] J. L. Agorreta, M. Borrega, J. López, and L. Marroyo, "Modeling and control of N-paralleled grid-connected inverters with LCL filter coupled due to grid impedance in PV plants," *IEEE Trans. Power Electron.*, vol. 26, no. 3, pp. 770–785, Mar. 2011.

[86] Y. Wang, Q. Xu, and G. Chen, "Simplified multi-modular shunt active power filter system and its modelling," *IET Power Electron.*, vol. 8, no. 6, pp. 967–976, 2015.

[87] C. Yu et al., "Modeling and resonance analysis of multiparallel inverters system under asynchronous carriers conditions," *IEEE Trans. Power Electron.*, vol. 32, no. 4, pp. 3192–3205, Apr. 2017.

[88] X. Zhang et al., "Modeling and resonance analysis of multi-paralleled grid-tied inverters in PV systems," *Proc. CSEE*, vol. 34, no. 3, pp. 336–345, 2014.

[89] J. Sun, "Small-signal methods for AC distributed power systems—A review," *IEEE Trans. Power Electron.*, vol. 24, no. 11, pp. 2545–2554, Nov. 2009.

[90] X. Chen and J. Sun, "A study of renewable energy system harmonic resonance based on a DG test-bed," in *Proc. IEEE 26th Annu. Appl. Power Electron. Conf. Expo.*, 2011, pp. 995–1002.

[91] Y. Hoon, M. A. M. Radzi, M. A. A. M. Zainuri, and M. A. M. Zawawi, "Shunt active power filter: A review on phase synchronization control techniques," *Electronics*, vol. 8, no. 7, 2019, Art. no. 791.

[92] J. Ma, X. Wang, F. Blaabjerg, L. Harnefors, and W. Song, "Accuracy analysis of the zero-order hold model for digital pulse width modulation," *IEEE Trans. Power Electron.*, vol. 33, no. 12, pp. 10826–10834, Dec. 2018.

[93] T. Itkonen, J. Luukko, A. Sankala, T. Laakkonen, and R. PÖllÄnen, "Modeling and analysis of the dead-time effects in parallel PWM two-level three-phase voltage-source inverters," *IEEE Trans. Power Electron.*, vol. 24, no. 11, pp. 2446–2455, Nov. 2009.

[94] J. Xu, X. Li, H. Liu, and X. Meng, "Fractional-order modeling and analysis of a three-phase voltage source PWM rectifier," *IEEE Access*, vol. 8, pp. 13507–13515, 2020.

[95] J. Xu, X. Li, X. Meng, J. Qin, and H. Liu, "Modeling and analysis of a single-phase fractional-order voltage source pulse width modulation rectifier," *J. Power Sources*, vol. 479, 2020, Art. no. 228821.

[96] X. Wei, C. Li, M. Qi, B. Luo, X. Deng, and G. Zhu, "Research on harmonic current amplification effect of parallel APF compensating voltage source nonlinear load," *Energies*, vol. 12, no. 16, 2019, Art. no. 3070.

[97] K. Dai, C. Liu, K. Duan, and Y. Kang, "Harmonic compensation characteristics of active power filters to nonlinear loads based on impedance analysis," in *Proc. IEEE Int. Symp. Ind. Electron.*, 2012, pp. 340–347.
[98] M. Liu et al., "Analysis and calculation on harmonic amplification effect of electric vehicle charging station using three-phase uncontrolled rectification charger," *Power Syst. Protect. Control*, vol. 44, no. 4, pp. 36–43, 2016.
[99] Y. Zhang, K. Dai, X. Chen, Y. Kang, and Z. Dai, "Stability analysis of SAPF by viewing DFT as cluster of BPF for selective harmonic suppression and resonance damping," *IEEE Trans. Ind. Appl.*, vol. 55, no. 2, pp. 1598–1607, Mar./Apr. 2019.
[100] X. Chen, K. Dai, C. Xu, L. Peng, and Y. Zhang, "Harmonic compensation and resonance damping for SAPF with selective closed-loop regulation of terminal voltage," *IET Power Electron.*, vol. 10, no. 6, pp. 619–629, 2017.
[101] C. Xu, K. Dai, X. Chen, L. Peng, Y. Zhang, and Z. Dai, "Parallel resonance detection and selective compensation control for SAPF with square-wave current active injection," *IEEE Trans. Ind. Electron.*, vol. 64, no. 10, pp. 8066–8078, Oct. 2017.
[102] D. Xu, F. Wang, Y. Ruan, and H. Mao, "Output impedance modeling of grid-connected inverters considering nonlinear effects," in *Proc. IEEE 13th Workshop Control Model. Power Electron.*, 2012, pp. 1–7.
[103] F. Wang, J. L. Duarte, M. A. Hendrix, and P. F. Ribeiro, "Modeling and analysis of grid harmonic distortion impact of aggregated DG inverters," *IEEE Trans. Power Electron.*, vol. 26, no. 3, pp. 786–797, Mar. 2011.
[104] J. Sun, "Impedance-based stability criterion for grid-connected inverters," *IEEE Trans. Power Electron.*, vol. 26, no. 11, pp. 3075–3078, Nov. 2011.
[105] M. Lu, X. Wang, F. Blaabjerg, and P. C. Loh, "An analysis method for harmonic resonance and stability of multi-paralleled LCL-filtered inverters," in *Proc. IEEE 6*th *Int. Symp. Power Electron. Distrib. Gener. Syst.*, 2015, pp. 1–6.
[106] M. Lu, X. Wang, P. C. Loh, and F. Blaabjerg, "Resonance interaction of multiparallel grid-connected inverters with LCL filter," *IEEE Trans. Power Electron.*, vol. 32, no. 2, pp. 894–899, Feb. 2017.
[107] P. Dang, J. Petzoldt, and T. Ellinger, "Stability analysis of multi-parallel APF systems," in *Proc. 14*th *Eur. Conf. Power Electron. Appl.*, 2011, pp. 1–8.
[108] S. Zhang, K. Dai, B. Xie, and Y. Kang, "Parallel control of shunt active power filters in capacity proportion frequency allocation mode," *J. Power Electron.*, vol. 10, no. 4, pp. 419–427, 2010.
[109] K. Liu, W. Cao, J. You, Y. Huang, J. Zhao, and J. Song, "Improved parallel operation for multi-modular shunt APF using dual harmonic compensation loop," in *Proc. IEEE 8th Int. Power Electron. Motion Control Conf.*, 2016, pp. 126–130.
[110] W. Yafang, G. Juping, C. Ruixiang, Q. Ling, and C. Juan, "The multi-modular shunt APF based on direct current control and frequency doubling carrier phase-shifted SPWM," in *Proc. IEEE ECCE Asia Downunder*, 2013, pp. 867–871.
[111] W. Cai, Y. Huang, F. Zhou, Q. Wu, H. Liu, and C. Wang, "Independent DC capacitance parallel multiple module SVG based on CPS-SPWM," in *Proc. IEEE 38th Annu. Conf. Ind. Electron. Soc.*, 2012, pp. 1350–1355.
[112] X. Bao, F. Zhuo, B. Liu, and Y. Tian, "Suppressing switching frequency circulating current in parallel inverters with carrier phase-shifted SPWM technique," in *Proc. IEEE Int. Symp. Ind. Electron.*, 2012, pp. 555–559.
[113] Z. Xi, Z. Xiao, and K. Li, "Design of master-slave active power filter control system based on concerto FPGA," in *Proc. 5th Int. Conf. Intell. Human-Mach. Syst. Cybern.*, 2013, pp. 470–473.
[114] M. S. El Moursi, H. Zeineldin, J. L. Kirtley, and K. Alobeidli, "A dynamic master/slave reactive power-management scheme for smart grids with distributed generation," *IEEE Trans. Power Del.*, vol. 29, no. 3, pp. 1157–1167, Jun. 2014.
[115] W. Wang, X. Zeng, X. Tang, and C. Tang, "Analysis of microgrid inverter droop controller with virtual output impedance under non-linear load condition," *IET Power Electron.*, vol. 7, no. 6, pp. 1547–1556, 2014.
[116] S. Leng, I.-Y. Chung, and D. A. Cartes, "Distributed operation of multiple shunt active power filters considering power quality improvement capacity," in *Proc. 2nd Int. Symp. Power Electron. Distrib. Gener. Syst.*, 2010, pp. 543–548.
[117] G. Falahi and H. Mokhtari, "Performance improvement of parallel active power filters using droop control method," in *Proc. Asia-Pacific Power Energy Eng. Conf.*, 2009, pp. 1–4.
[118] D. Chen, L. Xiao, H. Lian, and Z. Xu, "A fault tolerance method based on switch redundancy for shunt active power filter," *Energy Rep.*, vol. 7, pp. 449–457, 2021.
[119] Q.-W. Xu, J.-X. Zhan, L. Xiao, and G.-Z. Chen, "A multi-modular shunt active power filter system and its novel fault-tolerant strategy based on split-phase control and real-time bus communication," *Front. Inf. Technol. Electron. Eng.*, vol. 19, no. 9, pp. 1166–1179, 2018.
[120] W. Yifan, Y. Qing, G. Jinlong, Z. Hongyan, and X. Qunwei, "A fault redundancy strategy between bridge arms of the modularized APF," in *Proc. 12th IET Int. Conf. AC DC Power Transmiss.*, 2016, pp. 1–5.

Zhaokang Wu received the M.Sc. degree in electrical engineering from the Dalian University of Technology, Dalian, China, in 2020. He is currently working toward the Ph.D. degree in electrical engineering with the Department of Electrical Engineering, Shanghai University, Shanghai, China.

His research during the leader's program, from 2017 to 2020, focused on solid-state Marx generators and wireless power transmission. Since 2020, he has been actively involved in research related to power quality. His current research interests include active power filters, static VAR compensators, and resonance suppression in power electronic systems.

Guoqing Xu (Senior Member, IEEE) received the B.Sc., M.Sc., and Ph.D. degrees in electrical engineering from Zhejiang University, Hangzhou, China, in 1988, 1991, and 1994, respectively.

In 1997, he joined Tongji University, Shanghai, China, where he was a Professor with the Department of Electrical Engineering from 2000 to 2016. Since 2007, he has been a Research Professor and the Director of the Institute of CAS–CUHK Shenzhen Advanced Integration Technology, The Chinese University of Hong Kong, Hong Kong. Since 2016, he has been the Chief Scientist of the Center for Automotive Electronics, Shenzhen Institutes of Advanced Technology, Chinese Academy of Sciences, Shenzhen. He is currently a Professor and the Director of the Institute of Electrical and Control Engineering, Shanghai University, Shanghai. His research interests include electric vehicle control, motor drive and energy processing, and automotive electronics.

Wei Zhu received the B.Sc. degree from Hunan University, Changsha, China, in 1993, and the Ph.D. degree from Shanghai University, Shanghai, China, in 1998, respectively, both in electrical engineering.

From 1997 to 2005, he was the Technical Director of Robincom USA, China. Since 2005, he had been the General Manager of IPER. Since 2010, he had been the Vice-President of Shanghai Guangdian Electric Group Company Ltd., Shanghai. He is currently the Adjunct Professor and Ph.D. Supervisor of the Institute of Electrical and Control Engineering, Shanghai University, and the General Manager of Shanghai Nancal Electric Company Ltd., Shanghai. His research interests include vector control inverter, large-capacity high-voltage inverter, and quality of electric energy.

Gang Sheng received the M.Sc. degree in electrical engineering from Shanghai Jiao Tong University, Shanghai, China, in 2005.

In 2017, he joined the Department of Control System, Nancal Electric, Shanghai, China, as the Director. He has been involved in engineering practices related to power quality and motor drives for an extended period. He has led and participated in the design and research of multiple high-voltage inverters and active power filters. His research interests include high-performance control algorithms and industrial application technologies for power quality and motor drive systems.